

Distributed Multi-object Tracking under Limited Field of View Sensors

Hoa Van Nguyen, Hamid Rezatofighi, Ba-Ngu Vo, and Damith C. Ranasinghe

Abstract—We consider the challenging problem of tracking multiple objects using a distributed network of sensors. In the pragmatic settings of a limited field of view (FoV) sensors, computing and communication resources of nodes, we develop a novel *distributed multi-target algorithm* that fuses local multi-object states instead of local multi-object densities. This algorithm uses a novel *label consensus approach* that reduces label inconsistency, caused by movements of objects from one node's limited FoV to another. To accomplish this, we formalise the concept of label consistency and determine a sufficient condition to achieve it. The proposed algorithm is i) fast and requires significantly less processing time than fusion methods using multi-object filtering densities, and ii) achieves better tracking accuracy by considering tracking errors measured by the Optimal Sub-Pattern Assignment (OSPA) metric over several scans rather than a single scan. Numerical experiments demonstrate the real-time capability of our proposed solution, in computational efficiency and accuracy compared to state-of-the-art solutions in challenging scenarios.

Index Terms—Multi-sensor multi-object tracking, distributed multi-object tracking, label consistency, track consensus.

I. INTRODUCTION

Multi-Object Tracking (MOT) problems aim to estimate an unknown and time-varying number of object trajectories from noisy sensor measurements. Multi-object tracking is an integral component of a multitude of application domains, including radar surveillance [1], robotics [2], [3], computer vision [4], traffic monitoring [5], [6], cell biology [7], [8], and space exploration [9]. For many practical applications, sensor networks comprising of interconnected sensor *nodes* with sensing (for object detection), communication and processing capabilities, have attracted considerable research interest, driven by progress in wireless communication and sensing technologies [10]–[12].

Importantly, the provision of multiple sensing nodes addresses the practical and critical problem of limited observability of sensing modalities from a single node for tracking objects distributed across large spatial regions [9]. For example, the tracking of space debris using a network of low-earth-orbit cube satellites [13]. Sensor networks enable the inference

of more accurate trajectories by *fusing information* of multi-objects from observations at individual nodes (with limited observability) in a scalable (with respect to the number of nodes), flexible and reliable (*i.e.*, resilient to failures) manner [14]. Leveraging these benefits requires the sensor network to operate in a distributed mode, in so-called *distributed sensor networks*, where each node operates independently without any knowledge of the network topology whilst reaching consensus on multiple objects under surveillance.

Due to the significant benefits of distributed sensor networks for multi-object tracking applications, distributed MOT (DMOT) has attracted growing interest from researchers in recent years. MOT is a challenging problem itself; in addition to uncertainty from process and measurement noise, simultaneously tracking multiple objects are complicated by false-alarms, misdetections, data association uncertainty, and time-varying number of objects [15]. DMOT is a nontrivial problem and engages further complications. In particular, a suitable fusion algorithm is required to combine *common information* associated with an object to achieve improved tracking accuracy whilst merging *complementary information* to overcome the limited field of view of a sensor node.

In principle, optimal fusion can be achieved by preserving marginal and joint multi-object distributions from all nodes [16]. However, maintaining these distributions requires the sharing of common information among all nodes [10], [17], which limits the flexibility and scalability of the network. To maintain flexibility and scalability, robust (but sub-optimal) fusion solutions have been developed to address the double-counting of information when the common information is unknown [18].

Recent fusion techniques for DMOT were mostly developed from the random finite set framework because it facilitates principled generalisation of (single-object) distributed estimation to the multi-object case [17]. This framework offers a convenient notion of multi-object (probability) density that enabled the development of a suite of multi-object filters, *e.g.*, the probability hypothesis density (PHD) [19], cardinalised PHD (CPHD) [20], multi-Bernoulli (MB) [15], [21], [22], and labelled multi-Bernoulli (LMB) [23], generalised labelled multi-Bernoulli (GLMB) [24], [25], and multi-scan GLMB [26] filters. Many of these filters have been adapted for distributed multi-object estimation via the concept of Generalised Covariance Intersection (GCI¹) [17], [32], *e.g.*, PHD-GCI [18], CPHD-GCI [10], MB-GCI [33], LMB-GCI [34],

Acknowledgement: This work is supported by the Australian Research Council under Linkage Project LP160101177 and Discovery Project DP160104662.

Hoa Van Nguyen and Damith C. Ranasinghe are with the School of Computer Science, The University of Adelaide, SA 5005, Australia (e-mail: hoavan.nguyen,damith.ranasinghe@adelaide.edu.au).

Hamid Rezatofighi is with the Department of Data Science & AI, Monash University, Clayton VIC 3800, Australia (e-mail: hamid.rezatofighi@monash.edu).

Ba-Ngu Vo is with the Department of Electrical and Computer Engineering, Curtin University, Bentley, WA 6102, Australia (e-mail: ba-ngu.vo@curtin.edu.au).

¹GCI is also known as Chernoff fusion [27], [28], Exponential Mixture Density [18], [29], [30] or Kullback-Leibler Average [10], [11], [31]

and its variations [12], [35], [36].

When the nodes do not *share the same Field of View (FoV)*, which is invariably the case with distributed sensor networks, GCI-based filters tend to perform poorly [37]. A remedy for the PHD-GCI filter was proposed using cluster analysis (CA-PHD-GCI) [38]. However, this approach requires sharing FoV information among nodes and does not generate *object labels (identities)*, an important function of an MOT algorithm [1]. Labelled GCI-based filters generate object labels but tend to suffer from label inconsistency (*i.e.*, individual objects are assigned different labels by different nodes). While there are efforts to reduce label inconsistency for sensors *without FoV limitations* [12], [35], [36], the *more practical problems of reaching label consensus and reducing label inconsistency in distributed fusion with limited FoV sensors have not been addressed*. In addition to GCI, which is based on log-linear geometric averaging of probability densities, the linear arithmetic average has also been explored in the PHD [39], [40], CPHD [41], and MB filter [42]. However, the arithmetic averaging consensus for DMOT has not yet been developed.

While current fusion algorithms based on multi-object densities offer elegant conceptual solutions, these methods require intensive computing resources and high communication bandwidth. Due to the combinatorial nature of MOT, each multi-object distribution is characterised by a very large number of parameters. The computing resources needed to calculate these parameters at the nodes, and the bandwidth needed for communicating them to neighbouring nodes can be prohibitive for real-time DMOT with increasing numbers of networked nodes and objects [43]. The high computational time and bandwidth requirements can be circumvented by considering the distributed fusion of local multi-object states instead of multi-object densities. Although, track-to-track fusion and association algorithms investigated previously in [44]–[51] may offer a potential solution, these methods assume no false tracks nor missed objects, *i.e.*, the number of local tracks from any two nodes are the same [50]. This assumption is not pragmatic in problems involving a time-varying number of objects, and networks with limited FoV sensors.

In this work, we propose an *efficient* distributed fusion algorithm for DMOT considering practical limitations imposed by computing and communication resources as well as sensors with *different and limited FoVs*. Our solution fuses local multi-object states and employs a *novel label consensus* algorithm that reduces inconsistency in the estimated labels caused by objects moving from one node's limited FoV to another. The optimal solution to this problem is NP-hard (for more than 2 nodes). Considering real-time requirements of practical applications, we propose a tractable sub-optimal fusion solution that reduces label inconsistency. This strategy incurs far less computation time and bandwidth than multi-object filtering density-based solutions. It also achieves better tracking accuracy by considering the tracking errors over several scans using the Optimal Sub-Pattern Assignment⁽²⁾ (OSPA⁽²⁾) metric [52]–[54]. We also formalise the concept of label consistency and derive a sufficient condition to achieve label consistency by exploiting the metric properties of the OSPA⁽²⁾. To validate

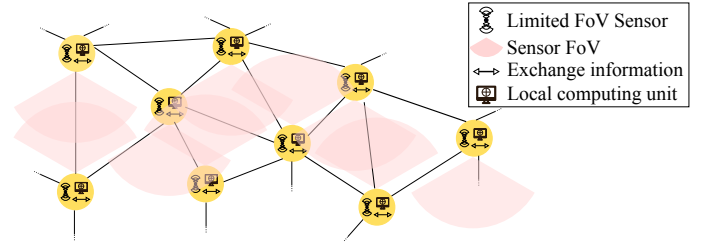


Fig. 1. A distributed sensor network system with limited FoVs.

the effectiveness of our proposed method, we benchmark its accuracy and fusing time against state-of-the-arts GCI-based solutions in a series of numerical experiments.

The paper is organised as follows. We define the problem and provide background on metrics in Section II. Section III presents our proposed fusion method. Section IV details numerical experiments, results and comparisons with GCI-based methods. Section V discusses concluding remarks.

II. BACKGROUND

This section provides the necessary background on distributed sensor network and multi-object error metrics.

A. Distributed sensor network description

Fig. 1 depicts a distributed heterogeneous network described by an undirected graph $\mathcal{G} = (\mathcal{N}, \mathcal{A})$, where \mathcal{N} is the set of nodes and $\mathcal{A} \in \mathcal{N} \times \mathcal{N}$ is the set of arcs representing connections among nodes. An arc $(a, b) \in \mathcal{A}$ means that node a can receive data from node b and vice-versa. We denote by $\mathcal{N}^{(a)} \triangleq \{b \in \mathcal{N} : b \neq a \text{ and } (a, b) \in \mathcal{A}\}$ the set of neighbours of node a from which data can be obtained. Each node is typically assigned with a unique ID. The set of all such IDs forms an ordered set (*e.g.*, integers), and is assumed to be known by all the nodes.

Consider the task of monitoring a large area using the network of Fig. 1 to detect and track an unknown and time-varying number of mobile objects. We assume that each node is equipped with a local computing unit capable of, computing local multi-object states, as well as a transceiver for communicating reliably with their neighbours through a limited range-and-bandwidth communication channel. In this context, a typical ad-hoc network exists between the nodes where each node can communicate its local multi-object state to other nodes directly or indirectly. Each node is equipped with a limited field-of-view (FoV) sensor subjected to false-alarms and misdetections. The network of interest has no central fusion node, and its nodes operate without knowledge of the network topology.

At time k , an existing object is represented by a *labelled state* $\mathbf{x}_k = (x_k, \ell_k)$, where $x_k \in \mathbb{X}$ is its *state vector*, and $\ell_k \in \mathbb{L}$ is a unique label consisting of the time of birth and an index to distinguish objects born at the same time. The set $\mathbf{X}_k \subset \mathbb{X} \times \mathbb{L}$ of labelled states of existing objects (with distinct labels) is called the *labelled multi-object state* (the set $X_k \subset \mathbb{X}$ of states of existing objects is called the *multi-object state*). We use the notation $|X|$ for the cardinality of a set X ,

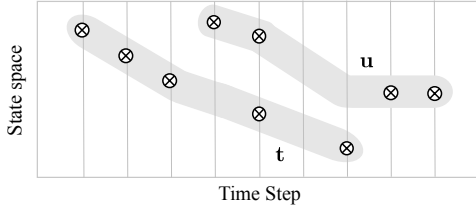


Fig. 2. A set of two fragmented tracks \mathbf{t} and \mathbf{u} .

and $\mathcal{L}(\mathbf{X}) = \{\mathcal{L}(\mathbf{x}) : \mathbf{x} \in \mathbf{X}\}$ for the set of labels of a multi-object state \mathbf{X} , where $\mathcal{L} : \mathbb{X} \times \mathbb{L} \rightarrow \mathbb{L}$ is the label projection defined by $\mathcal{L}((x, \ell)) = \ell$.

Given a (discrete) time interval $\mathbb{K} \triangleq \{1, \dots, K\}$ from the start time at 1 to the end time at K of the scenario, let \mathbb{T} denote the space of all functions $t : \mathbb{K} \rightarrow \mathbb{X}$. An element $t \in \mathbb{T}$ is called a *track*, and a *labelled track* \mathbf{t} is an ordered pair $(t, \ell) \in \mathbb{T} \times \mathbb{L}$. The set $\mathcal{D}^{(\mathbf{t})} \subseteq \mathbb{K}$ of time instances that the track $\mathbf{t} = (t, \ell)$ exists is the domain $\mathcal{D}^{(\mathbf{t})}$ of t , and the labelled state vector at time $k \in \mathcal{D}^{(\mathbf{t})}$ is given by $\mathbf{x}_k = (t(k), \ell)$. We also use the same notation for the label projection $\mathcal{L}((t, \ell)) = \ell$, and $\mathcal{L}(\mathbf{T}) = \{\mathcal{L}(\mathbf{t}) : \mathbf{t} \in \mathbf{T}\}$, for $\mathbf{T} \subset \mathbb{T} \times \mathbb{L}$. Further, let $\mathcal{T} : \mathbb{T} \times \mathbb{L} \rightarrow \mathbb{T}$ be the track projection defined by $\mathcal{T}((t, \ell)) = t$ and $\mathcal{T}(\mathbf{T}) = \{\mathcal{T}(\mathbf{t}) : \mathbf{t} \in \mathbf{T}\}$.

Two remarks are in order. Firstly, the definition of labelled tracks meets the MOT requirement that tracks should have *labels (or identities)* [1]. Secondly, the set $\mathcal{D}^{(\mathbf{t})}$ of instances that track \mathbf{t} exists need not be consecutive (see Fig. 2), and hence encompasses the so-called *fragmented tracks* generated by many MOT algorithms. A *fragmented track* arises when the MOT algorithm declares it to be non-existent (possibly due to misdetections) in between instances where it (is declared to) exist as illustrated in Fig. 2. When $\mathcal{D}^{(\mathbf{t})}$ consists of consecutive instances, track \mathbf{t} is called a *trajectory*.

Given a finite set $\mathbf{T} \subset \mathbb{T} \times \mathbb{L}$ of labelled tracks with distinct labels, the labelled multi-object state at time $k \in \mathbb{K}$ is given by $\mathbf{X}_k = \cup_{(t, \ell) \in \mathbf{T}} \{(t(k), \ell)\}$. Note that the history $\mathbf{X}_{1:K} \triangleq \mathbf{X}_1, \dots, \mathbf{X}_K$ of labelled multi-object states completely determines the set \mathbf{T} , and hence we use the notation $\mathbf{X}_{1:K}$ to denote the set of labelled tracks on the interval \mathbb{K} . We denote the restriction of the track t , labelled track \mathbf{t} , and set of labelled tracks $\mathbf{X}_{1:K}$ (or \mathbf{T}) on the window $\{j : k\} \subset \mathbb{K}$, by $t_{j:k}$, $\mathbf{t}_{j:k}$, and $\mathbf{X}_{j:k}$ (or $\mathbf{T}_{j:k}$). Hereon, the discussions in this paper only concern the time window $\{j : k\}$, hence, for notational compactness, we drop the subscript $j : k$ when no confusion arises, e.g., $\mathbf{T} \triangleq \mathbf{T}_{j:k}$.

Instead of seeking consensus amongst local multi-object densities as pursued in many of the latest works [12], [38], we are interested in reaching consensus amongst local multi-object states from the set \mathcal{N} of nodes. At time k , each local node a communicates a message which is an ordered pair (a, \mathbf{X}_k) comprising of the node's identity a and the local labelled multi-object state \mathbf{X}_k . Let $\mathbb{L} = \mathbb{L} \times \mathcal{N}$ be the global label space of the network, wherein each global label is unique across the network. Let $\mathbf{X}_k^{(a)} = \{(x, (\ell, a)) : (x, \ell) \in \mathbf{X}_k\} \subset \mathbb{X} \times \mathbb{L}$ be the globally labelled multi-object state of node a at time k generated from the communicated message (a, \mathbf{X}_k) , and $\mathbb{L}_k^{(a)} = \mathcal{L}(\mathbf{X}_k^{(a)}) = \{\ell \triangleq (\ell, a) : \ell \in \mathcal{L}(\mathbf{X}_k)\} \subset \mathbb{L}$

be its corresponding set of global labels. The receiving node (e.g., $b \in \mathcal{N}^{(a)}$) stores $\mathbf{X}_k^{(a)}$ in its own memory to form a set of globally labelled tracks $\mathbf{X}^{(a)}$ (or $\mathbf{T}^{(a)} \subset \mathbb{T} \times \mathbb{L}$) from node a . Given the sets of globally labelled track estimates $\{\mathbf{T}^{(a)}\}_{a \in \mathcal{N}}$, our objective is to compute a consensed globally labelled multi-object state estimate $\mathbf{X}_k^{\text{con}} \subset \mathbb{X} \times \mathbb{L}$ by reaching a consensus on the latest labelled multi-object state estimates $\{\mathbf{X}_k^{(a)}\}_{a \in \mathcal{N}}$ in terms of kinematic and labels. Moreover, we seek an efficient algorithm that is scalable with respect to (wrt) network size.

Our solution is based on minimising the overall dissimilarity of tracks between sensor nodes. We employ a metric to measure such dissimilarities. Thus, in the next subsection, we revisit the metric property and a widely used metric in evaluating the tracking performance of MOT algorithms.

B. Multi-object metrics

A function $d : \mathcal{S} \times \mathcal{S} \rightarrow [0, \infty)$ is called a *metric* or a *distance* function on the space \mathcal{S} if it meets the following conditions:

- 1) $d(x, y) = 0$ if and only if $x = y$ (identity),
- 2) $d(x, y) = d(y, x)$ (symmetry),
- 3) $d(x, y) \leq d(x, z) + d(z, y)$ (triangle inequality).

We are interested in distances between two finite subsets $X = \{x^{(1)}, \dots, x^{(m)}\}$ and $Y = \{y^{(1)}, \dots, y^{(n)}\}$ of a space equipped with a metric d , referred to as the base-distance (between the elements of X and Y). An example of particular relevance to this work is the Optimal Sub-Pattern Assignment (OSPA) metric.

Let $d^{(c)}(x, y) \triangleq \min(c, d(x, y))$, and Π_n be the set of all permutations of $\{1, 2, \dots, n\}$. The OSPA metric of (integer) order $p \geq 1$ and cut-off $c \in (0, \infty)$ is defined as [55]:

$$d_0^{(p,c)}(X, Y) = \left(\frac{1}{n} \left(\min_{\pi \in \Pi_n} \sum_{i=1}^m d^{(c)}(x^{(i)}, y^{(\pi(i))})^p + c^p(n-m) \right) \right)^{1/p}, \quad (1)$$

if $m \leq n$, and $d_0^{(p,c)}(X, Y) \triangleq d_0^{(p,c)}(Y, X)$, if $m > n$, in addition, $d_0^{(p,c)}(X, Y) = c$ if one of the argument is empty, and $d_0^{(p,c)}(\emptyset, \emptyset) = 0$. The two adjustable parameters p , and c , are interpreted as the outlier and cardinality sensitivities, respectively. The OSPA metric can be interpreted as the best-case localisation and cardinality error per object.

Given a meaningful base-distance $d^{(c)}(\cdot, \cdot)$ between two tracks, the OSPA metric provides meaningful distances between two finite subsets of tracks. One such base-distance is the time-averaged OSPA distance between the states of two tracks over time instances when at least one of the tracks exists [54]. Specifically, for any $t, u \in \mathbb{T}$,

$$\tilde{d}^{(c)}(t, u) = \sum_{k \in \mathcal{D}^{(t)} \cup \mathcal{D}^{(u)}} \frac{d_0^{(c)}(\{t(k)\}, \{u(k)\})}{|\mathcal{D}^{(t)} \cup \mathcal{D}^{(u)}|} \quad (2)$$

if $\mathcal{D}^{(t)} \cup \mathcal{D}^{(u)} \neq \emptyset$, and $\tilde{d}^{(c)}(t, u) = 0$, if $\mathcal{D}^{(t)} \cup \mathcal{D}^{(u)} = \emptyset$, where $d_0^{(c)}(\{t(k)\}, \{u(k)\})$ denotes the OSPA distance, and since the arguments are only sets of at most one element, the

parameter p no longer comes into play. We call this distance the *OSPA track-to-track distance*.

The OSPA metric with OSPA track-to-track distance in (2), called OSPA-on-OSPA or $\text{OSPA}^{(2)}$, provides a natural distance between two sets of tracks. This distance can be interpreted as the time-averaged per-track error and demonstrates meaningful behaviour on various MOT scenarios. Errors in localisation, cardinality, track fragmentation and track identity switching, all yield intended increases in the $\text{OSPA}^{(2)}$ error. The higher the frequency of track fragmentation and identity switches, the higher the $\text{OSPA}^{(2)}$ error. A dropped track that later regained with the same identity yields a smaller increase in $\text{OSPA}^{(2)}$ error than if it were regained with a different identity [54].

III. FUSION USING TRACK CONSENSUS

In this section, we present a novel algorithm for fusing the latest local labelled multi-object state estimates among the distributed network of sensor nodes. Our innovation is based on measuring the dissimilarity of tracks between nodes over multiple scans (*i.e.*, time window) instead of relying on the multi-object densities at a single scan as in previous works. Fusing multi-object state estimates instead of multi-object densities significantly reduces the processing time and bandwidth. Moreover, the proposed solution is applicable to non-overlapping or partially overlapping limited FoVs of sensor nodes and improves tracking accuracy as well as cardinality estimations (or *detectability* of objects).

We first consider the problem of measuring the dissimilarity between tracks. For this purpose, we define optimal track matching via the OSPA track-to-track distance. Based on the notion of optimal track matching, we formalise the concept of label consistency and derive a sufficient condition to achieve it. We then develop a novel algorithm for *track consensus* by: *i*) formulating a method for achieving kinematic consensus between track estimates made by two nodes (Section III-C); *ii*) extending this to a pair-wise fusion algorithm for kinematic consensus when the number of nodes are greater than two (Section III-D); and *iii*) developing a label consensus algorithm to achieve label consistency across the distributed network of nodes (Section III-E).

A. Optimal track matching

Consider two nodes $a, b \in \mathcal{N}$. Without loss of generality, suppose that fusion is performed at node a . At time k , the aim is to compute a consensed labelled multi-object state $\mathbf{X}_k^{(a, \text{con})}$ at node a from $\mathbf{X}_k^{(a)}$ and $\mathbf{X}_k^{(b)}$. Since $\mathbf{X}_k^{(a, \text{con})}$ is computed from the latest local labelled multi-object states, previously terminated tracks have no influence, only tracks declared to *exist* at k are considered. With a slight abuse of notation, let $\mathbf{T}_k^{(a)} = \{\mathbf{t} \in \mathbf{T}^{(a)} : \mathcal{L}(\mathbf{t}) \in \mathcal{L}(\mathbf{X}_k^{(a)})\}$ be the set of live tracks at k , as declared by node a , truncated on the window $[j : k]$, and likewise for $\mathbf{T}_k^{(b)} = \{\mathbf{t} \in \mathbf{T}^{(b)} : \mathcal{L}(\mathbf{t}) \in \mathcal{L}(\mathbf{X}_k^{(b)})\}$. For notational compactness, we use the shorthand $a^{(m)} = \mathcal{T}(\mathbf{a}^{(m)})$, $b^{(m)} = \mathcal{T}(\mathbf{b}^{(m)})$, and $u^{(m)} = \mathcal{T}(\mathbf{u}^{(m)})$.

Definition 1. Given two sets of tracks $\mathbf{T}_k^{(a)} = \{\mathbf{a}^{(1)}, \dots, \mathbf{a}^{(|\mathbf{T}_k^{(a)}|)}\}$ and $\mathbf{T}_k^{(b)} = \{\mathbf{b}^{(1)}, \dots, \mathbf{b}^{(|\mathbf{T}_k^{(b)}|)}\}$, assuming that $|\mathbf{T}_k^{(a)}| \leq |\mathbf{T}_k^{(b)}|$. We define the optimal matching as

the pairing of elements between the two sets that yields the $\text{OSPA}^{(2)}$ distance $d_0^{(1, c)}(\mathcal{T}(\mathbf{T}_k^{(a)}), \mathcal{T}(\mathbf{T}_k^{(b)}))$ *i.e.*,

$$\pi^* = \arg \min_{\pi \in \Pi_{|\mathbf{T}_k^{(b)}|}} \sum_{m=1}^{|\mathbf{T}_k^{(a)}|} \tilde{d}^{(c)}(a^{(m)}, b^{(\pi(m))}), \quad (3)$$

Here, $\pi^*(m) = n$ means track $\mathbf{a}^{(m)} \in \mathbf{T}_k^{(a)}$ is matched to track $\mathbf{b}^{(n)} \in \mathbf{T}_k^{(b)}$.

The optimal assignment problem can be solved using the Hungarian algorithm [56], [57] with $\mathcal{O}(|\mathbf{T}_k^{(b)}|^4)$ complexity, or using efficient algorithms in [58]–[60] with $\mathcal{O}(|\mathbf{T}_k^{(b)}|^3)$ complexity.

Remark 1. The processing time of the optimal assignment in (3) is considerably shorter than LM-GCI proposed in [12] where each node runs an LMB filter. The reason is that for the LMB filter, the multi-object state is extracted from the LMB density for any labels with existence probabilities higher than a predefined threshold (typically 0.5). Thus, the label space of the multi-object state used in (3) is substantially smaller than the label space of the LMB density used in LM-GCI.

B. Label consistency and performance bound

In this subsection, we formalise the concept of label consistency for the consensus of labelled tracks. Note that while the term label consistency/inconsistency has been used in the context of DMOT in [35], there is no formal definition.

Definition 2. Let $\mathbf{u}^{(1)}, \dots, \mathbf{u}^{(N)} \in \mathbb{T} \times \mathbb{L}$ be the true trajectories of N distinct objects. Let $\mathbf{a}^{(1)}, \dots, \mathbf{a}^{(N)}$ be their corresponding track estimates at node a , and $\mathbf{b}^{(1)}, \dots, \mathbf{b}^{(N)}$ be their corresponding track estimates at node b . Then, we say that label consistency is achievable when the optimal matching π^* between these sets of track estimates satisfies

$$\pi^*(m) = m, \quad \forall m \in \{1, \dots, N\}. \quad (4)$$

Moreover, suppose that for each $m \in \{1, \dots, N\}$ the tracks $\mathbf{a}^{(m)}$ and $\mathbf{b}^{(m)}$ are assigned new labels, resulting in tracks $\bar{\mathbf{a}}^{(m)}$ and $\bar{\mathbf{b}}^{(m)}$. Then, we say label consistency is achieved if

$$\mathcal{L}(\bar{\mathbf{a}}^{(m)}) = \mathcal{L}(\bar{\mathbf{b}}^{(m)}), \quad \forall m \in \{1, \dots, N\}. \quad (5)$$

Remark 2. Definition 2 can be easily extended to more than two nodes. Suppose that $\bar{\mathbf{t}}^{(1)}, \dots, \bar{\mathbf{t}}^{(|\mathcal{N}|)}$ $\in \mathbb{T} \times \mathbb{L}$ are the globally labelled track estimates of a true trajectory \mathbf{u} . Then label consistency is achieved if

$$\mathcal{L}(\bar{\mathbf{t}}^{(m)}) = \mathcal{L}(\bar{\mathbf{t}}^{(n)}), \quad \forall m, n \in \{1, \dots, |\mathcal{N}|\}. \quad (6)$$

The following result provides the conditions to achieve label consistency (see Appendix A for proofs).

Proposition 1. Consider the trajectories $\mathbf{u}^{(1)}, \dots, \mathbf{u}^{(N)}$ of $N \leq \min(|\mathbf{T}_k^{(a)}|, |\mathbf{T}_k^{(b)}|)$ distinct objects. Let us denote their corresponding labelled track estimates at nodes a and b , by $\mathbf{a}^{(1)}, \dots, \mathbf{a}^{(N)}$ and $\mathbf{b}^{(1)}, \dots, \mathbf{b}^{(N)}$. Suppose that their track-to-track errors $\tilde{d}^{(c)}(a^{(m)}, u^{(m)})$, $\tilde{d}^{(c)}(u^{(m)}, b^{(m)})$ at nodes a and b , are bounded by \mathcal{E} for all $m \in \{1, \dots, N\}$, and that:

$$\begin{aligned} \tilde{d}^{(c)}(a^{(m)}, b^{(n)}) &= c \quad \forall m > N, \forall n \in \{1, \dots, |\mathbf{T}_k^{(b)}|\}, \\ \tilde{d}^{(c)}(a^{(m)}, b^{(n)}) &= c \quad \forall m \in \{1, \dots, |\mathbf{T}_k^{(a)}|\}, \forall n > N. \end{aligned} \quad (7)$$

Then, to achieve label consistency for these N distinct objects, we need

$$\tilde{d}^{(c)}(u^{(m)}, u^{(n)}) > 4\mathcal{E} \quad \forall m, n \in \{1, \dots, N\}, m \neq n. \quad (8)$$

For a given upper bound on the track-to-track error, the above result provides a lower bound on the separation of the true trajectories required to achieve label consistency. A conservative track-to-track error bound can be determined from the kinematic error, and the frequency of misses or alternatively, the empirical existence probability.

Definition 3. The empirical existence probability of a track t over the time interval $\{j : k\}$ is defined as

$$P_X(t) = \frac{|\mathcal{D}^{(t)}|}{k - j + 1}, \quad (9)$$

where $\mathcal{D}^{(t)} \subseteq \{j : k\}$ is the domain of track t .

Proposition 2. Let P_X^{\min} be minimum empirical existence probabilities of all tracks at nodes a and b , i.e.,

$$P_X^{\min} = \min_{\mathbf{t} \in \mathbf{T}_k^{(a)} \cup \mathbf{T}_k^{(b)}} P_X(\mathcal{T}(\mathbf{t})), \quad (10)$$

Suppose the single-scan estimation errors at nodes a and b are bounded as follows:

$$\begin{aligned} d_0^{(c)}(\{a^{(m)}(i)\}, \{u^{(m)}(i)\}) &= \begin{cases} c & i \notin \mathcal{D}^{(\mathbf{a}^{(m)})} \\ d^{(c)}(a^{(m)}(i), u^{(m)}(i)) \leq \varepsilon & i \in \mathcal{D}^{(\mathbf{a}^{(m)})} \end{cases}, \\ d_0^{(c)}(\{b^{(m)}(i)\}, \{u^{(m)}(i)\}) &= \begin{cases} c & i \notin \mathcal{D}^{(\mathbf{b}^{(m)})} \\ d^{(c)}(b^{(m)}(i), u^{(m)}(i)) \leq \varepsilon & i \in \mathcal{D}^{(\mathbf{b}^{(m)})} \end{cases}, \\ \forall m \in \{1, \dots, N\}. \end{aligned}$$

Then the track-to-track error is bounded by

$$\varepsilon P_X^{\min} + c(1 - P_X^{\min}). \quad (11)$$

Remark 3. If the window $[j : k]$ is long enough, and a “good” multi-object tracker (e.g., MHT [61], GLMB [24], [25] or multi-scan GLMB [26]) is used, then it is possible to have $P_X^{\min} \geq P_D$ where P_D is the detection probability. Further, the single-scan estimation error bound ε is often proportional to Frobenius norm $\|R\|_F$ of the measurement noise covariance R . Empirically, we observe that $\varepsilon = 2\|R\|_F \leq c$, thus:

$$\varepsilon P_X^{\min} + c(1 - P_X^{\min}) \leq 2P_D\|R\|_F + c(1 - P_D), \quad (12)$$

and the condition for label consistency is

$$\begin{aligned} \tilde{d}^{(c)}(u^{(m)}, u^{(n)}) &> 4[2P_D\|R\|_F + c(1 - P_D)], \\ \forall m, n \in \{1, \dots, N\}, m \neq n. \end{aligned} \quad (13)$$

Intuitively, (13) suggests that label consistency can be achieved when *i)* the object true trajectories are reasonably well-separated, *ii)* the measurement noise covariance R is fairly small, *iii)* the detection probability P_D is relatively high.

C. Kinematic consensus for two nodes

Since each node is equipped with a limited FoV sensor, only track estimates within the overlapped FoV of two sensors (observed² by both nodes’ FoVs) should be matched and

fused to enhance tracking accuracy. Further, the unmatched tracks (outside the overlapped FoV of two sensors) should be retained to improve detectability. Thus, the set of tracks at each node can be divided into three subsets: *i)* matched tracks, *ii)* unmatched and retained tracks, *iii)* unmatched and discarded tracks. However, for distributed sensor networks, the sensor FoV information of other nodes is usually unknown, and we rely on the separation between two-track estimates to determine if they are matched or not. For all pairs (m, n) such that $\pi^*(m) = n$, only pairs with associated costs $C_{m,n} = \tilde{d}^{(c)}(a^{(m)}, b^{(n)})$ less than a predefined threshold $\mathcal{C}_{\text{match}}$ are considered matched. A small $\mathcal{C}_{\text{match}}$ can lead to a smaller number of matched pairs which results in a higher number of unmatched tracks (possibly false tracks) and vice versa. Since the maximum value of $C_{m,n}$ is the cut-off c in (1), $\mathcal{C}_{\text{match}}$ should not be greater than c . In particular, let $Q_k = [Q_k^{(a)}, Q_k^{(b)}]$ be a two-column matrix contains all matched pairs indexes (m, n) such that

$$\begin{aligned} m \in Q_k^{(a)} &\subseteq \{1, \dots, |\mathbf{T}_k^{(a)}|\}, \\ n \in Q_k^{(b)} &\subseteq \{1, \dots, |\mathbf{T}_k^{(b)}|\}, \\ \text{subject to } \pi^*(m) &= n, C_{m,n} < \mathcal{C}_{\text{match}}. \end{aligned} \quad (14)$$

The steps for determining matched pairs is given in Algorithm B.1 (see Appendix B).

For the unmatched tracks, some of these can be false tracks and should be discarded. Thus, we propose that only unmatched tracks with lengths higher than a predefined track length \mathcal{C}_{len} are retained. Similar to the traditional thresholding method in extracting raw measurements, a small track length \mathcal{C}_{len} helps to detect new objects faster with a higher number of false-positive tracks and vice versa [62]. As a result, the consensed labelled multi-object state comprises of two components: *i)* the matched and fused labelled states, *ii)* the unmatched and retained labelled states of two nodes. In summary, kinematic fusion steps are:

Step 1) Fuse matched labelled states: We compute³ the set $\bar{\mathbf{X}}_k^{(a)}$ of matched labelled states at node a by fusing matched labelled states, i.e.,

$$\bar{\mathbf{X}}_k^{(a)} = \{(x, \ell^{(m)}) : x = w^{(a)}a^{(m)}(k) + w^{(b)}b^{(n)}(k), (m, n) \in Q_k\}, \quad (15)$$

where $w^{(a)}$ and $w^{(b)}$ be the fusing weights of two nodes with $w^{(a)} + w^{(b)} = 1$ and $w^{(a)}, w^{(b)} > 0$ (See (21) later in Section IV for how the weights are selected).

Step 2) Retain unmatched labelled states: We retain the set $\mathbf{X}_k^{(a, \text{ret})}$ of unmatched labelled states at node a (likewise for $\mathbf{X}_k^{(b, \text{ret})}$ at node b) whose lengths exceed a given \mathcal{C}_{len} , i.e.,

$$\mathbf{X}_k^{(a, \text{ret})} = \{\mathbf{a}^{(m)}(k) : m \in \{1, \dots, |\mathbf{T}_k^{(a)}|\} \setminus Q_k^{(a)}, |\mathcal{D}^{(\mathbf{a}^{(m)})}| \geq \mathcal{C}_{\text{len}}\}. \quad (16)$$

Further, any unmatched tracks with lengths less than \mathcal{C}_{len} are discarded.

²When we say track t is observed at node a means that node a declares track t exist.

³We implement a naive solution here such that the fused label is the label of the node performing the fusion steps while further improvements to achieve label consensus are discussed in Section III-E.

3) *Compute consensed labelled states*: We compute the set $\mathbf{X}_k^{(a,\text{con})}$ of consensed labelled states at node a by combining two components: *i*) the matched and fused labelled states, *ii*) the unmatched and retained labelled states of two nodes, *i.e.*,

$$\mathbf{X}_k^{(a,\text{con})} = \bar{\mathbf{X}}_k^{(a)} \cup \mathbf{X}_k^{(a,\text{ret})} \cup \mathbf{X}_k^{(b,\text{ret})}. \quad (17)$$

Remark 4. The consensed labelled multi-object state $\mathbf{X}_k^{(a,\text{con})}$ does not play a role in optimal matching at the next time step and is used for reporting purposes only. The local multi-object state $\mathbf{X}_{k+1}^{(a)}$ at the next time step $k+1$ is independent of $\mathbf{X}_k^{(a,\text{con})}$. The optimal matching at $k+1$ only depends on sets of live tracks $\mathbf{T}_{k+1}^{(a)}$ and $\mathbf{T}_{k+1}^{(b)}$, not on the consensed multi-object state $\mathbf{X}_k^{(a,\text{con})}$.

The overall procedure for fusing two nodes is provided in Algorithm 1. This algorithm maintains a $|\mathbf{L}_{1:k}^{(a)}| \times |\mathbf{L}_{1:k}^{(b)}|$ *matched history* matrix $\Xi_{1:k}^{(a,b)}$ (line 4) whose elements are the number of instances track $i^{(m)} \in \{1, \dots, |\mathbf{L}_{1:k}^{(a)}|\}$ is matched with track $i^{(n)} \in \{1, \dots, |\mathbf{L}_{1:k}^{(b)}|\}$. Here, $\mathbf{L}_{1:k}^{(a)}$ is the label space up to time k at node a (likewise for $\mathbf{L}_{1:k}^{(b)}$ at node b). See Algorithm B.2 in Appendix B for more details.

Algorithm 1 FuseTwoNodes

Input: $\mathbf{T}_k^{(a)}, \mathbf{T}_k^{(b)}, \Xi_{1:k-1}^{(a,b)}, \mathbf{L}_{1:k-1}^{(a)}, \mathbf{L}_{1:k-1}^{(b)}, C_{\text{len}}$;
Output: $\mathbf{X}_k^{(a,\text{con})}, \Xi_{1:k}^{(a,b)}, \mathbf{L}_{1:k}^{(a)}, \mathbf{L}_{1:k}^{(b)}$;
1: $\mathbf{L}_{1:k}^{(a)} = \mathbf{L}_{1:k-1}^{(a)} \cup (\mathcal{L}(\mathbf{T}_k^{(a)}) \setminus \mathbf{L}_{1:k-1}^{(a)})$;
2: $\mathbf{L}_{1:k}^{(b)} = \mathbf{L}_{1:k-1}^{(b)} \cup (\mathcal{L}(\mathbf{T}_k^{(b)}) \setminus \mathbf{L}_{1:k-1}^{(b)})$;
3: $Q_k := \text{DetermineMatchedPairs}(\mathbf{T}_k^{(a)}, \mathbf{T}_k^{(b)})$;
4: $\Xi_{1:k}^{(a,b)} := \text{UpdateMatchedHistory}(\Xi_{1:k-1}^{(a,b)}, \mathbf{L}_{1:k-1}^{(a)}, \mathbf{L}_{1:k-1}^{(b)}, Q_k)$;
5: Compute $\bar{\mathbf{X}}_k^{(a)}$ via (15); $\mathbf{X}_k^{(a,\text{ret})}$ and $\mathbf{X}_k^{(b,\text{ret})}$ via (16);
6: $\mathbf{X}_k^{(a,\text{con})} := \bar{\mathbf{X}}_k^{(a)} \cup \mathbf{X}_k^{(a,\text{ret})} \cup \mathbf{X}_k^{(b,\text{ret})}$;

D. Kinematic consensus for multiple nodes

The previous subsections presented a new kinematic consensus algorithm for fusing multi-object states between two nodes. We now extend the algorithm to more than two nodes. A direct extension results in an $|\mathcal{N}|$ -dimensional optimal assignment for the track matching, which is an NP-hard problem. A widely used sub-optimal strategy to circumvent this intractable problem is to perform pair-wise matching sequentially [10], [12], [31]. Based on the proposed network architecture in Section II-A, kinematic consensus is realised in Algorithm 2, which is called TC-OSPA⁽²⁾. Algorithm 2 consists of two steps: *Step 1) Fuse each neighbour node with current node*: Each neighbour labelled multi-object state is fused to the labelled multi-object state of the node of interest to ensure that only unmatched labelled states with the track lengths greater than or equal to C_{len} are retained.

Step 2) Fuse the consensed labelled states sequentially: The consensed labelled states of neighbouring nodes and the nodes of interest are combined sequentially without the track length constraint (*i.e.*, $C_{\text{len}} = 1$) to retain all unmatched tracks because the label consensus has not been reached.

Algorithm 2 (TC-OSPA⁽²⁾) can be implemented in real-time given the significantly low message sizes realised by

Algorithm 2 FuseMultiNodes

Input: $\{\mathbf{T}_k^{(a)}\}_{a \in \mathcal{N}}; \{\Xi_{1:k-1}^{(a,b)}\}_{a,b \in \mathcal{N}}; \{\mathbf{L}_{1:k-1}^{(a)}\}_{a \in \mathcal{N}}$;
Output: $\{\mathbf{X}_k^{(a,\text{con})}\}_{a \in \mathcal{N}}; \{\Xi_{1:k}^{(a,b)}\}_{a,b \in \mathcal{N}}; \{\mathbf{L}_{1:k}^{(a)}\}_{a \in \mathcal{N}}$;
1: **for** $a = 1 : |\mathcal{N}|$ **do**
2: $\mathcal{B} := \{1 : |\mathcal{N}| \setminus \{a\}\}$;
3: $\mathbf{X}_{\text{temp}} = \emptyset$; \triangleright Temporarily consensed labelled multi-object state.
4: **for** $i = 1 : |\mathcal{B}|$ **do**
5: \triangleright Step 1: fuse each neighbour node with current node.
6: $b := \mathcal{B}(i)$;
7: $[\mathbf{X}_{\text{temp}}^{(i)}, \Xi_{1:k}^{(a,b)}, \mathbf{L}_{1:k}^{(a)}, \mathbf{L}_{1:k}^{(b)}] :=$
8: $\text{FuseTwoNodes}(\mathbf{T}_k^{(a)}, \mathbf{T}_k^{(b)}, \Xi_{1:k-1}^{(a,b)}, \mathbf{L}_{1:k-1}^{(a)}, \mathbf{L}_{1:k-1}^{(b)}, C_{\text{len}})$;
9: **end for**
10: $\mathbf{X}_k^{(a,\text{con})} := \mathbf{X}_{\text{temp}}^{(1)}$;
11: **if** $|\mathcal{B}| > 1$ **then**
12: \triangleright Step 2: fuse the consensed labelled states sequentially.
13: **for** $i = 2 : |\mathcal{B}|$ **do**
14: $\mathbf{X}_k^{(a,\text{con})} := \text{FuseTwoNodes}(\mathbf{X}_k^{(a,\text{con})}, \mathbf{X}_{\text{temp}}^{(i)}, \emptyset, \emptyset, \emptyset, 1)$;
15: **end for**
16: $\mathbf{L}_{a,k}^{\text{con}} := \text{UpdateLabels}(\mathcal{L}(\mathbf{X}_k^{(a,\text{con})}); \{\Xi_{1:k}^{(a,b)}\}_{a,b \in \mathcal{N}}; \{\mathbf{L}_{1:k}^{(a)}\}_{a \in \mathcal{N}})$;
17: **end for**

transmitting labelled multi-object states compared to transmitting labelled multi-object densities. In particular, suppose that $|\mathbf{T}_{\text{max}}|$ is the maximum number of objects seen by the network, *i.e.*, $|\mathbf{T}_{\text{max}}| = \max(|\mathbf{T}^{(1)}|, \dots, |\mathbf{T}^{(|\mathcal{N}|)}|)$, then the order of magnitude of data that needs to be shared is upper bounded by⁴

$$|\mathcal{N}| |\mathbf{T}_{\text{max}}|. \quad (18)$$

For example, if $|\mathcal{N}| = 20$ nodes, $|\mathbf{T}_{\text{max}}| = 100$ objects, and each labelled object state has 6 dimensions (4 for 2D environments of kinematic state and 2 for the local label's dimension), and each dimension is represented by an 8-byte floating-point value, then the maximum amount of data that needs to be shared by a node at one time is 96 KB, which is reasonably low to track a large number of objects using 20 distributed nodes. See numerical experiments in Sec. IV for fusing time.

E. Label consensus for multiple objects

The previous subsections address multiple limited FoVs *kinematic consensus*. However, MOT concerns not only the object's positions (kinematic) but also the object's identities (labels). In this subsection, we present our *label consensus* solution that reduces the occurrences of label inconsistency. During the fusion steps, the unmatched and retained labelled states are included in the consensed labelled multi-object state (see (17)). Hence, care must be taken to ensure mismatched labels between nodes are resolved to achieve *label consensus* as illustrated in the following example.

Example 1. Consider using a two-node distributed sensor network to track a mobile object that follows a constant velocity model over a $[-500, 1500] \text{m} \times [0, 1000] \text{m}$ area. The locations of the two nodes are $[0, 400]^T \text{m}$ and $[0, 800]^T \text{m}$,

⁴The upper bound is only reached in the case that all nodes observe all the objects. In reality, because of limited FoV sensors, this upper bound will not be reached in most cases.

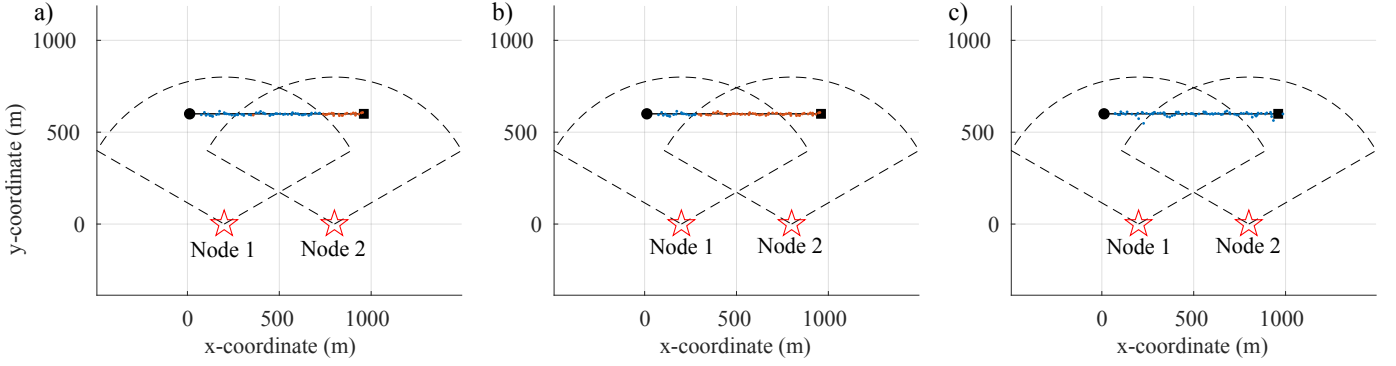


Fig. 3. Example 1 — two nodes with limited FoVs tasked with tracking a single object. a) Consensed labelled state at node 1 before reaching label consensus; b) Consensed labelled state at node 2 before reaching label consensus; c) Consensed labelled state at node 1 (likewise for node 2) after reaching label consensus. Here: ‘o’ is the location of the object’s birth; ‘□’ is the location of the object’s death. Colour coding represents labels of the objects.

respectively. Each node runs an LMB filter locally, and its sensor can only detect objects within its relative angle $[-60^\circ, 60^\circ]$ with detection probability $P_D = 0.98$ and detection range $r_D = 800$ m (see Fig. 3). After the kinematic consensus steps, we have the two following label inconsistency problems:

1) *Label inconsistency of the unmatched and retained labelled states.* Fig. 3a depicts the consensed labelled state at node 1. Although the kinematic fusion successfully helps node 1 track the object, even when it moves out of node 1’s FoV, a track fragmentation still occurs. This happens because it is no longer detected by node 1 and the network relies on detection information from node 2 (including node 2’s label) to track it. Since node 2 has a different label (in red) to the one observed by node 1 (in blue), the consensed labelled state yields two different labels for the same object.

2) *Label inconsistency of the matched labelled states.* Fig. 3b depicts the consensed labelled state at node 2. Initially, the object is not detected by node 2; hence, the network relies on the information from node 1 (including node 1’s label in blue) to track it. When the object moves into node 2’s FoV, node 2 assigns it a new label in red. During the fusion steps (see (15)), the object is assigned the red label of node 2 (since the fusion is performed at node 2). As a result, the consensed labelled state has different labels for the same object.

In the following, we present a label consensus solution to reduce label inconsistency. The main idea is to construct a graph that represents connections among labels based on the match history matrices $\Xi_{1:k}^{(a,b)}$ whose (m, n) entry is the number of instances the m th track in node a ’s track-list is matched with the n th track in node b ’s track-list. In particular, let $G = (V, E)$ be a graph, where:

- the set V of labels is the set of vertices of the graph;
- E is the set of edges representing matches between labels.

Since label consistency requires the same object to have the same label across all nodes of the network (Remark 2), all of the connected vertices should be assigned the same label. For this so-called consensed label, we propose to use the least label of connected vertices according to a lexicographical order of

time of birth and unique node ID :

$$\begin{aligned} \ell = ((k, i), a) < \ell' = ((k', i'), b) \\ \Leftrightarrow (k = k') \text{ and } (a < b) \text{ or } (k < k'). \end{aligned} \quad (19)$$

The proposed label consensus is provided in Algorithm B.3 in Appendix B, which is used in line 15 of Algorithm 2. Fig. 3c depicts the consensed labelled multi-object state at node 1 after label consensus is achieved. Observe that label inconsistency is eliminated.

IV. NUMERICAL EXPERIMENTS

In this section, we apply the proposed TC-OSPA⁽²⁾ fusion method to investigate and compare with other fusion strategies in three distributed sensor network settings of increasing complexity. A 2-dimensional search area is adopted for these three scenarios to demonstrate the effectiveness of our method. Each detected object with kinematic state $x = [p_x, \dot{p}_x, p_y, \dot{p}_y]^T$ results in an observation z of noisy xy -coordinate positions, given by: $z = [p_x, p_y]^T + v$. Here, $v \sim N(0, R)$ is a 2×1 zero-mean Gaussian process noise with $R = \text{diag}(\sigma_x^2, \sigma_y^2)$ where $\sigma_x = \sigma_y = 10$ m. Each object follows a constant velocity model given by $x_k = F^{CV} x_{k-1} + q_{k-1}^{CV}$. Here, $F^{CV} = [1, T_0; 0, T_0] \otimes I_2$, T_0 is the sampling interval ($T_0 = 1$ s for our experiments), \otimes denotes for the Kronecker tensor product; I_2 is the 2×2 identity matrix; $q_{k-1}^{CV} \sim N(0, Q^{CV})$ is a 4×1 zero-mean Gaussian process noise, with co-variance $Q^{CV} = \sigma_{CV}^2 [T_0^3/3, T_0^2/2; T_0^2/2, T_0] \otimes I_2$ where $\sigma_{CV} = 5$ m/s². Each object has a survival probability $P_S = 0.98$. Clutter follows a Poisson model with an average of 10 clutters per scan. We use OSPA and OSPA⁽²⁾ as well as fusing time to measure performance. For OSPA and OSPA⁽²⁾, we set cut-off $c = 100$ m, order $p = 1$. The OSPA⁽²⁾ distance at time k is calculated over a 10-scan window ending at k . The fusing time reported is the average execution time for the fusion steps over 100 MC runs—notably, this excludes the execution of the filtering algorithm.

For a fair comparison with LM-GCI in [12], we use an LMB filter at each local node, *although our approach can be applied with different filters*. The LMB filter is implemented with Gaussian mixtures using Gibbs sampling [63] for a joint prediction and update step. The existence threshold is set at 10^{-3} , *i.e.*, any Bernoulli component with label ℓ

and its existence probability $r^{(\ell)} < 10^{-3}$ is pruned. Any Bernoulli component with label ℓ and its existence probability $r^{(\ell)} > 0.5$ is confirmed as an existing object and extracted as a state with label ℓ . Further, we implement the Adaptive Birth Procedure (ABP) in [23]. In particular, the birth distribution $\pi_{B,k+1}$ at time $k+1$ is a function of measurement sets Z_k , i.e., $\pi_{B,k+1} = \{r_{B,k+1}^{(\ell)}(z), p_{B,k+1}^{(\ell)}(x|z)\}_{\ell=1}^{|Z_k|}$, where

$$r_{B,k+1}^{(\ell)}(z) = \min \left(r_{B,\max}, \frac{1 - r_{U,k}(z)}{\sum_{\zeta \in Z_k} 1 - r_{U,k}(\zeta)} \lambda_{B,k+1} \right).$$

Here, $r_{U,k}(z)$ is the probability that the measurement z is associated to track hypotheses, given by

$$r_{U,k}(z) = \sum_{I_{k-1}, \xi, I_k, \theta_k} 1_{\theta_k}(z) w^{(I_{k-1}, \xi)} w^{(I_k, \theta_k)}, \quad (20)$$

where $w^{(I_{k-1}, \xi)} w^{(I_k, \theta_k)}$ is in [63, eq.14], $\lambda_{B,k+1}$ is the expected number of births at time $k+1$ and $r_{B,\max}$ is the maximum existence probability of a newly born object. In three scenarios, we set $\lambda_{B,k+1} = 0.5$ and $r_{B,\max} = 0.03$.

For data fusion, since we do not focus on the weight selection problem, the Metropolis weight [64] is implemented, i.e., for each node $a, b \in \mathcal{N}$,

$$w^{(a,b)} = \begin{cases} \frac{1}{1 + \max(|\mathcal{N}^{(a)}|, |\mathcal{N}^{(b)}|)}, & a \in \mathcal{N}, b \in \mathcal{N}^{(a)}, \\ 1 - \sum_{b \in \mathcal{N}^{(a)}} w^{(a,b)}, & a \in \mathcal{N}, b = a. \end{cases} \quad (21)$$

The cost threshold for determining matched pairs is set at $C_{\text{match}} = 100$ m, which is equal to cut-off c .

We compare the proposed fusion method, TC-OSPA⁽²⁾, with CA-PHD-GCI [38] and LM-GCI [12]. We also compare our proposed approach with the OSPA metric replaced by the Wasserstein metric, here on referred to as TC-WASS. The Wasserstein metric of (integer) order $p \geq 1$ is defined as [65]:

$$d_W^{(p)}(X, Y) \triangleq \min_{\bar{C}} \left(\sum_{i=1}^m \sum_{j=1}^n \bar{C}_{i,j} d(x^{(i)}, y^{(j)})^p \right)^{1/p} \quad (22)$$

where $\bar{C} = (\bar{C}_{i,j})$ denotes an $m \times n$ transportation matrix, i.e., the entries $\bar{C}_{i,j}$ are non-negative, each row sum to $1/m$, and each column sum to $1/n$. The integer p determines the sensitivity of the metric to outliers in the finite subsets X and Y . Notably, the Wasserstein distance is undefined if one of the finite subsets is empty. Consequently, unlike the OSPA track-to-track distance in (2), the time-average (track-to-track) Wasserstein distance between two tracks is undefined if one track is fragmented (as shown in Fig. 2). One method to define a Wasserstein track-to-track distance is to embed the time information as a part of multi-object states: for any $t, u \in \mathbb{T}$, we form finite sets $\tilde{X}^{(t)} = \{(t(k), \alpha k) : k \in \mathcal{D}^{(t)}\}$ and $\tilde{X}^{(u)} = \{(u(k), \alpha k) : k \in \mathcal{D}^{(u)}\}$ and define

$$\tilde{d}_W(t, u) = d_W^{(p)}(\tilde{X}^{(t)}, \tilde{X}^{(u)}), \quad (23)$$

where α is a user-defined parameter to calibrate the influence of time on the overall distance. In our experiments, we set $\alpha = 20$ m/s—the maximum velocity of all objects.

For the CA-PHD-GCI fusion strategy, the underlying PHD filter does not report labels for multi-object states; hence, the resulting OSPA⁽²⁾ cannot be computed. We propose the

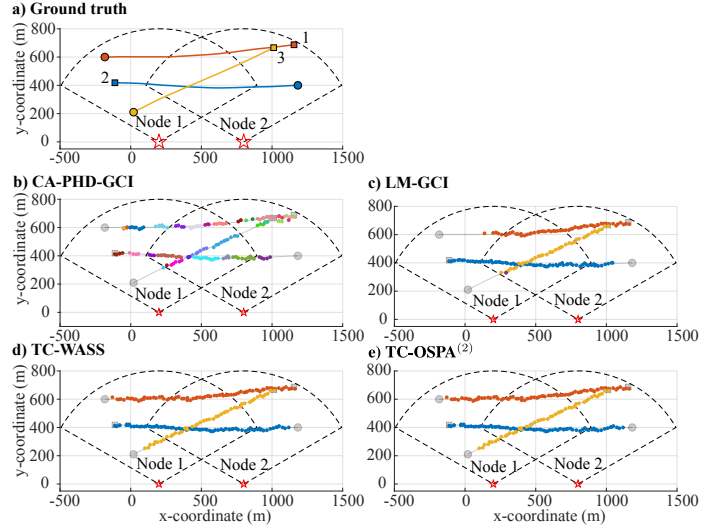


Fig. 4. Scenario 1 ground-truth and consensed labelled multi-object states at sensor node 2: a) ground-truth; b) CA-PHD-GCI; c) LM-GCI; d) TC-WASS; e) TC-OSPA⁽²⁾. Starting and stopping positions are denoted by \circ and \square , respectively. Colour coding represents labels of the objects.

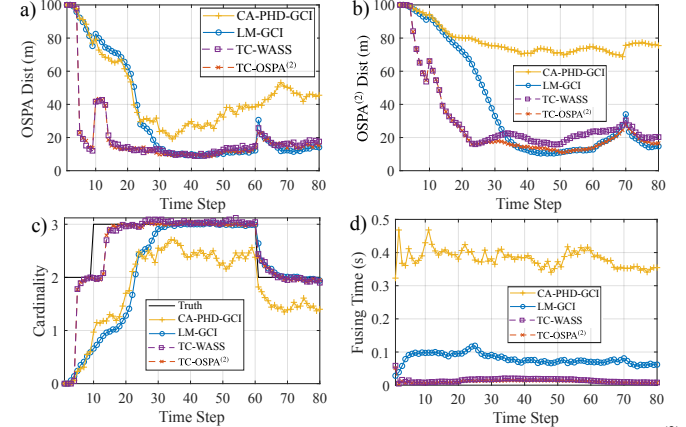


Fig. 5. Comparison results for Scenario 1: a) OSPA distance; b) OSPA⁽²⁾ distance; c) Cardinality estimations; d) Fusing times.

following naive label assignment approach for CA-PHD-GCI: *i)* match the multi-object state X_k to the previous multi-object state X_{k-1} using a similar scheme as Algorithm B.1 but with a track length threshold of 1 and OSPA distance instead of OSPA⁽²⁾; *ii)* assign the same labels for the matched multi-object state of X_k ; *iii)* assign newborn labels at time k for unmatched multi-object states of X_k .

A. Scenario 1 — two nodes with a small number of objects

In this setting, we investigate the simple problem of tracking three mobile objects using two sensor nodes with limited FoV sensors in a $[-500, 1500] \text{ m} \times [0, 800] \text{ m}$ area. The two nodes are located at $[0, 400]^T \text{ m}$ and $[0, 800]^T \text{ m}$, respectively. At each node, the sensor can only detect objects within its relative angle of $[-50^\circ, 50^\circ]$ with $P_D = 0.98$ and $r_D = 800$ m. The duration for this scenario is 80 s, with object 1 and object 2 staying alive for the whole period, while object 3 is born at time 10 s and dies at time 60 s. The track consensus is performed over 5 scans, with track length threshold $C_{\text{len}} = 2$, i.e., only unmatched tracks with lengths exceeding 2 are retained. The considered scenario setting is shown in Fig. 4a.

TABLE I
SCENARIO 1 RESULTS COMPARISON OVER 100 MONTE CARLO RUNS

Strategies	OSPA (m)	OSPA ⁽²⁾ (m)	Fusing time (s)
CA-PHD-GCI	46.6	78.2	0.383
LM-GCI	31.7	38.8	0.079
TC-WASS	19.6	29.7	0.013
TC-OSPA ⁽²⁾	19.0	27.0	0.011

Fig. 4, Fig. 5 and Table I compares results across CA-PHD-GCI, LM-GCI, TC-WASS and TC-OSPA⁽²⁾ fusion methods. The results confirm that our proposed TC-OSPA⁽²⁾ method can accurately detect and track all three objects with consistent labels whilst consuming the shortest fusing time. Due to the small number of objects, TC-WASS also attains a low OSPA error; however, TC-WASS occasionally fails to assign correct labels and results in a higher OSPA⁽²⁾ error as seen in Table I. In contrast, LM-GCI is only able to detect and track objects accurately within a sensor's own FoV. After the 30 s duration mark, all three objects are within the intersection of the two sensors' FoVs and we can observe Node 2 to correctly track all three objects as illustrated in Fig. 5a and 5c. Further, although CA-PHD-GCI can track most of these three objects, it cannot assign correct labels and we can observe a large degree of label inconsistency across the tracks.

B. Scenario 2 — two nodes with a large number of objects

In this scenario, we consider a more challenging problem using two limited-FoV sensor nodes to track a time-varying and unknown number of mobile objects in a $[-500, 1800] \text{ m} \times [-100, 1000] \text{ m}$ surveillance area. The two nodes are located at $[300, -100]^T \text{ m}$ and $[1000, -100]^T \text{ m}$, respectively. Each sensor can only detect objects within its limited FoV defined by a relative angle of interval $[-50^\circ, 50^\circ]$ with $P_D = 0.98$ and detection range $r_D = 1000 \text{ m}$. The duration of this scenario is 80 s, with various birth and death events, and a maximum of 22 objects. The track consensus between two nodes is performed over 5 scans, with track length threshold $\mathcal{C}_{\text{len}} = 2$. The considered scenario is illustrated in Fig. 6a.

Fig. 6b-d depict the consensed labelled multi-object states and the true trajectories at sensor node 2 of a particular run for CA-PHD-GCI, LM-GCI, TC-WASS and TC-OSPA⁽²⁾, respectively. The results confirm that TC-OSPA⁽²⁾ successfully detect and track all objects without any label inconsistency, regardless of whether objects are in the node's FoV or not. In contrast, LM-GCI can only detect and track most of the objects within the node's FoV. Although CA-PHD-GCI can detect all objects, even those outside the node's FoV, CA-PHD-GCI cannot determine the trajectories of objects. Fig 7c shows the cardinality estimates; the evidence therein further supports the above observation. It is expected that LM-GCI fails to detect all of the objects compared to CA-PHD-GCI, TC-WASS and TC-OSPA⁽²⁾ since only the latter three strategies are designed to cope with limited FoV sensors.

Fig. 7a-d and Table II present the performance comparisons among the four fusion strategies in terms of OSPA, OSPA⁽²⁾ and fusing time over 100 Monte Carlo runs. We can see that TC-OSPA⁽²⁾ outperforms other fusion strategies, including our

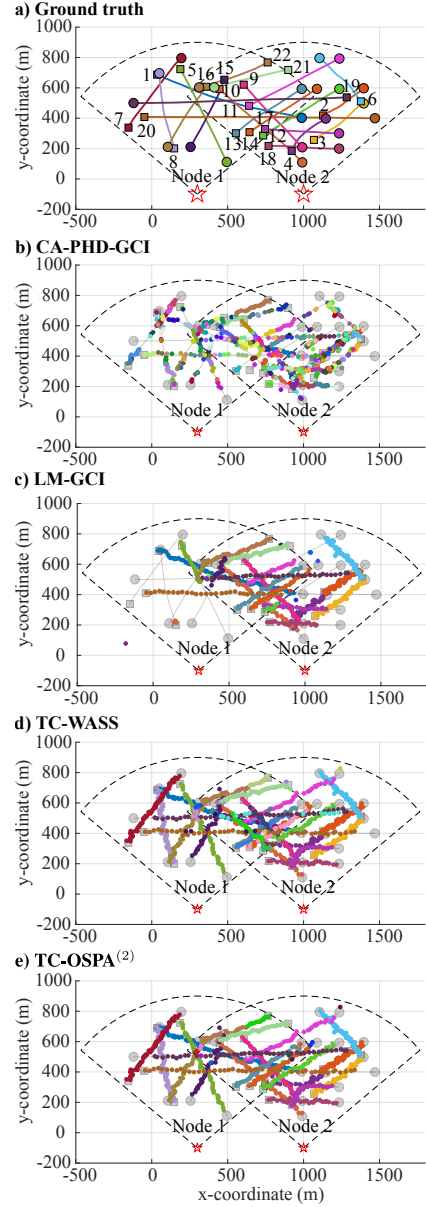


Fig. 6. Scenario 2 ground-truth and consensed labelled multi-object states at sensor node 2: a) ground-truth; b) CA-PHD-GCI; c) LM-GCI; d) TC-WASS; e) TC-OSPA⁽²⁾. Starting and stopping positions are denoted by \circ and \square , respectively. Colour coding represents labels of the objects. Although less apparent, there are several false tracks visible in the region of $[500, 1000] \text{ m} \times [200, 600] \text{ m}$ in Fig. 6d when using TC-WASS.

TABLE II
SCENARIO 2 COMPARISON RESULTS OVER 100 MONTE CARLO RUNS

Strategies	OSPA (m)	OSPA ⁽²⁾ (m)	Fusing time (s)
CA-PHD-GCI	51.5	87.9	1.095
LM-GCI	42.9	50.1	0.359
TC-WASS	28.6	45.6	0.078
TC-OSPA ⁽²⁾	21.0	32.5	0.052

track consensus fusion strategy employed with the adaptation of Wasserstein metric (TC-WASS), by large margins whilst requiring the shortest fusing time. The reason is that TC-OSPA⁽²⁾ minimises label inconsistency for limited FoV sensors while fusing the most certain object states within a sensor's FoV (local labelled multi-object states) to reach consensus in both position and label estimations.

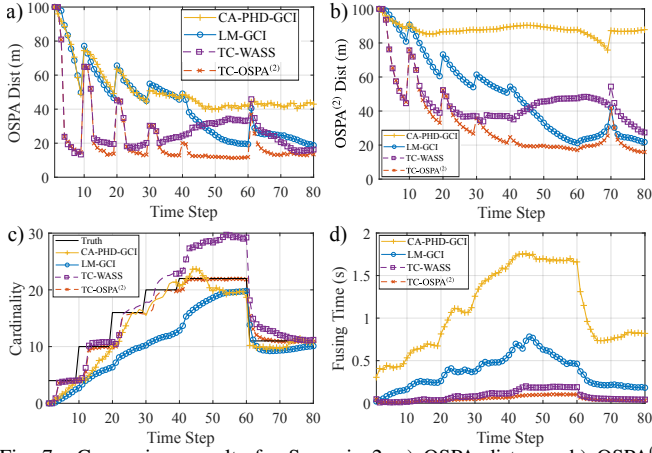


Fig. 7. Comparison results for Scenario 2: a) OSPA distance; b) OSPA⁽²⁾ distance; c) Cardinality estimations; d) Fusing times.

TABLE III

PERFORMANCE COMPARISON FOR DIFFERENT P_D VALUES OBTAINED OVER 100 MONTE CARLO RUNS FOR EACH P_D SETTING AND METHOD

	P_D	CA-PHD-GCI	LM-GCI	TC-WASS	TC-OSPA ⁽²⁾
OSPA (m)	0.7	78.9	61.1	39.9	37.1
	0.8	71.1	52.4	34.5	30.0
	0.9	64.4	44.7	31.1	24.1
OSPA ⁽²⁾ (m)	0.7	93.1	67.4	55.7	49.3
	0.8	90.6	59.6	51.8	42.4
	0.9	88.6	52.3	48.3	35.9

Table III further compares performance of TC-OSPA⁽²⁾ with LM-GCI, CA-PHD-GCI, and TC-WASS under different detection probability, P_D , settings. It is expected that the occurrences of label inconsistency will increase when P_D decreases. Consequently, the tracking accuracy decreases when P_D decreases; concurring with our observation in Remark 3. Nevertheless, the results in Table III show the proposed TC-OSPA⁽²⁾ approach to consistently outperform the other three fusion strategies across the P_D values.

C. Scenario 3 — a large number of nodes

To further demonstrate the effectiveness of our proposed fusion method, we consider a scenario with 16 limited FoV sensor nodes for tracking a time-varying and unknown number of mobile objects in a $[-1000, 1000] \text{ m} \times [-1000, 1000] \text{ m}$ surveillance area. These 16 nodes are positioned near the edge of the area. Each sensor can only detect objects within its limited FoV defined by a relative angle of interval $[-25^\circ, 25^\circ]$ with $P_D = 0.98$ and detection range $r_D = 1000 \text{ m}$. The duration of this scenario is 75 s with various birth, death events, and a maximum of 18 objects. Further, due to higher uncertainty, the track consensus is performed over 10 scans (instead of 5 as in Scenario 2), with a track length threshold $\mathcal{C}_{\text{len}} = 4$. The scenario described is depicted in Fig. 8a. Notably, for this scenario, we can only compare TC-OSPA⁽²⁾ with TC-WASS and LM-GCI since it is unclear how CA-PHD-GCI can be implemented for more than two nodes.

Fig. 8b-d depict the consensed labelled multi-object states and the ground-truth at node 7 for LM-GCI, TC-WASS and TC-OSPA⁽²⁾, respectively, for one particular execution.

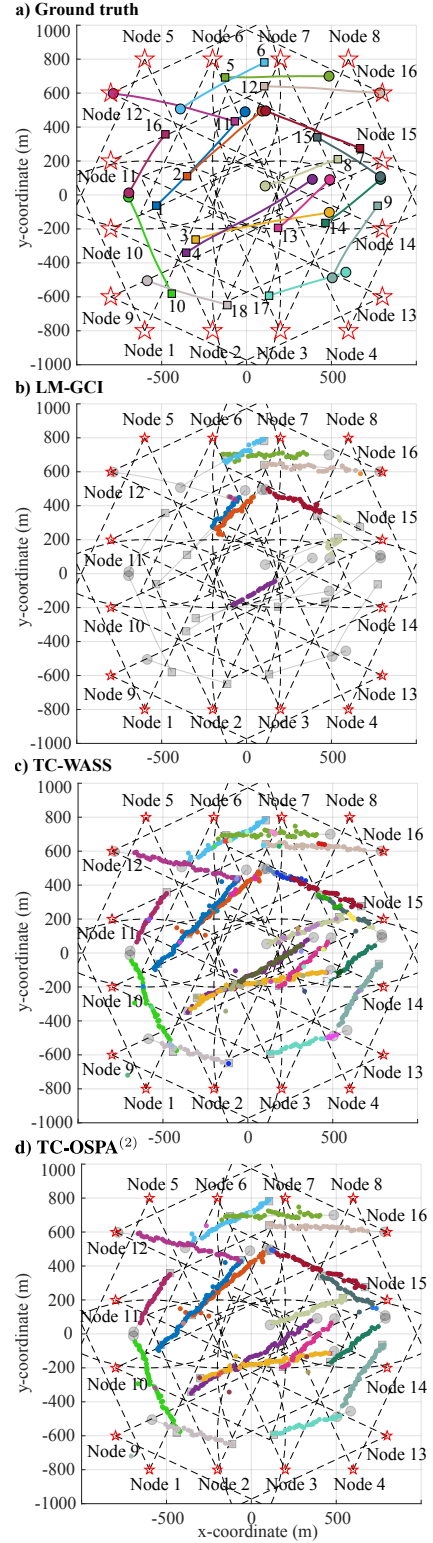


Fig. 8. Scenario 3 — ground-truth and consensed labelled multi-object states at sensor node 7: a) ground-truth; b) LM-GCI; c) TC-WASS; d) TC-OSPA⁽²⁾. Starting and stopping positions are denoted by \circ and \square , respectively. Colour coding represents labels of the objects.

Although LM-GCI detects a few objects outside of node 7's FoV, a considerable number of objects are missed because LM-GCI is not designed for partially overlapped sensor FoV situations. In contrast, TC-WASS and TC-OSPA⁽²⁾ employing our track consensus-based fusion method can detect, track and

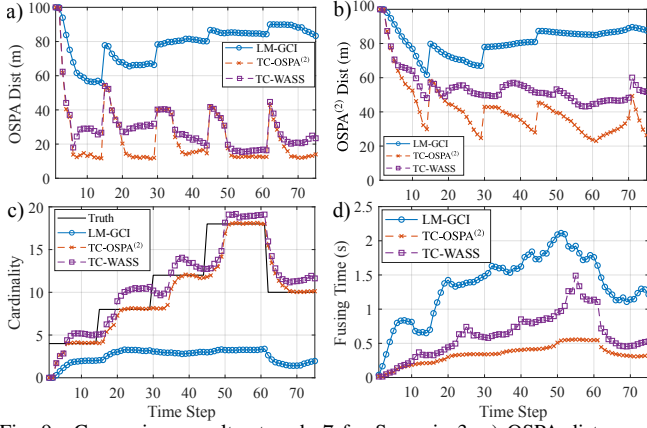


Fig. 9. Comparison results at node 7 for Scenario 3: a) OSPA distance; b) OSPA⁽²⁾ distance; c) Cardinality estimations; d) Fusing times.

TABLE IV
SCENARIO 3 COMPARISON RESULTS OVER 100 MONTE CARLO RUNS

Strategies	OSPA (m)	OSPA ⁽²⁾ (m)	Fusing times (s)
LM-GCI	78.7	81.6	1.35
TC-WASS	30.2	54.4	0.62
TC-OSPA ⁽²⁾	23.7	41.3	0.34

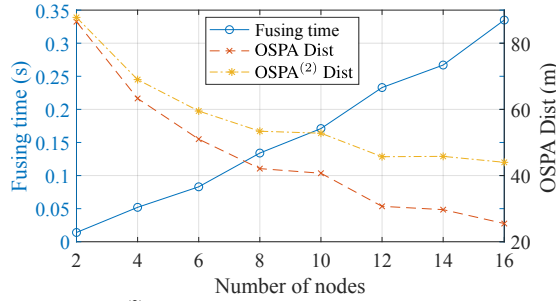


Fig. 10. TC-OSPA⁽²⁾ tracking performance at sensor node 2 for Scenario 3 over 100 MC runs when the number of nodes are increased from 2 to 16.

assign correct labels for most of the objects, regardless of the objects' locations. The results are further confirmed by the cardinality estimates plotted in Fig. 9c, which demonstrates that TC-OSPA⁽²⁾ and TC-WASS can detect and track all 18 objects in this scenario. In comparison, LM-GCI can only detect up to 4 objects on average, over 100 MC runs.

Fig. 9a-d provide detailed tracking performance comparisons, not easily visible in Fig. 8. The results further demonstrate the robustness of TC-OSPA⁽²⁾, it significantly outperforms LM-GCI and TC-WASS across three performance metrics: OSPA, OSPA⁽²⁾ and fusing time. Table IV summarises performance comparison results confirming the effectiveness of our proposed distributed fusion strategy.

Fig. 10 plots the overall tracking performance at sensor node 2 in Scenario 3 for TC-OSPA⁽²⁾ as the number of nodes are increased from 2 to 16. The results validate the scalability of our proposed fusion strategy, wherein the fusing time increases linearly with respect to the number of nodes, *i.e.*, $\mathcal{O}(|N|)$. Even with 16 nodes, the fusing time is relatively short, suitable for real-time tracking in several applications. As expected, when the number of nodes increases, OSPA and OSPA⁽²⁾ errors reduce since nodes can benefit shared local labelled multi-object states of other nodes to complement a node's own limited FoV, improve coverage area, and tracking accuracy.

V. CONCLUSION

A new scalable DMOT solution for multi-sensors with limited FoV sensors has been proposed. Our solution consists of a novel track consensus algorithm coupled with label consensus method based on the OSPA⁽²⁾ metric. The better efficiency and accuracy of the proposed DMOT solution are due to the fusion of multi-object state estimates using track consensus over several scans. In contrast, current solutions fuse multi-object densities from a single scan. Experimental results demonstrate improvements in both speed and accuracy over current methods.

Importantly, our DMOT approach does not rely on any specific tracking methodology but only requires that each node provide a set of estimated tracks. Hence different nodes of the network can execute different MOT algorithms, an advantage in heterogeneous and ad-hoc networks.

APPENDIX

A. Mathematical proofs

Proof of Proposition 1: For any $m \in \{1, \dots, N\}$, applying triangle inequality, we have:

$$\begin{aligned} \tilde{d}^{(c)}(a^{(m)}, b^{(m)}) &\leq \tilde{d}^{(c)}(a^{(m)}, u^{(m)}) + \tilde{d}^{(c)}(u^{(m)}, b^{(m)}), \\ &\leq 2\mathcal{E}. \end{aligned} \quad (24)$$

Similarly, using the triangle inequality and the bound \mathcal{E} , for any $n, m \in \{1, \dots, N\}$ and $n \neq m$, we have

$$\tilde{d}^{(c)}(a^{(m)}, b^{(n)}) \geq \tilde{d}^{(c)}(u^{(m)}, b^{(n)}) - \tilde{d}^{(c)}(u^{(m)}, a^{(m)}) \quad (25)$$

$$\begin{aligned} &\geq \tilde{d}^{(c)}(u^{(m)}, b^{(n)}) - \mathcal{E}, \\ &\geq \tilde{d}^{(c)}(u^{(m)}, u^{(n)}) - 2\mathcal{E}. \end{aligned} \quad (26)$$

Using (8) and $\tilde{d}^{(c)}(u^{(m)}, u^{(n)}) > 4\mathcal{E}$, we have

$$\tilde{d}^{(c)}(a^{(m)}, b^{(n)}) > \tilde{d}^{(c)}(a^{(m)}, b^{(m)}). \quad (27)$$

Using Definition 1 and (7), we have

$$\pi^* = \arg \min_{\pi \in \Pi_{|\mathbf{T}_k^{(b)}|}} \sum_{m=1}^{|\mathbf{T}_k^{(a)}|} \tilde{d}^{(c)}(a^{(m)}, b^{(\pi(m))}) \quad (28)$$

$$= \arg \min_{\pi \in \Pi_{|\mathbf{T}_k^{(b)}|}} \left[\sum_{m=1}^N \tilde{d}^{(c)}(a^{(m)}, b^{(\pi(m))}) + (|\mathbf{T}_k^{(a)}| - N)c \right]. \quad (29)$$

Since $\tilde{d}^{(c)}(a^{(m)}, b^{(\pi(m))}) = c \ \forall \pi(m) > N$ according to (7) and $(|\mathbf{T}_k^{(a)}| - N)c$ is a constant, (29) is equivalent to

$$\pi^* = \arg \min_{\pi \in \Pi_N} J(\pi), \quad (30)$$

where $J(\pi) = \sum_{m=1}^N \tilde{d}^{(c)}(a^{(m)}, b^{\pi(m)})$.

Let $\hat{\pi} \in \Pi_N$ be an assignment function that satisfies (4) (*i.e.*, $\hat{\pi}(m) = m \ \forall m \in \{1, \dots, N\}$). According to Definition 2, if π^* satisfies (4), and we assign the same label to each matched pair, then the N distinct objects have label consistency.

We now prove that $\pi^* = \hat{\pi}$ by using contradiction. Suppose that $\pi^* \neq \hat{\pi}$. Then according to (30), $J(\pi^*) < J(\hat{\pi})$. Thus, $\exists m, n \in \{1, \dots, N\}$ and $m \neq n$ such that $\pi^*(m) = n$ and

$\tilde{d}^{(c)}(a^{(m)}, b^{(n)}) \leq \tilde{d}^{(c)}(a^{(m)}, b^{(m)})$, otherwise we would have $J(\pi^*) > J(\hat{\pi})$. However, $\tilde{d}^{(c)}(a^{(m)}, b^{(n)}) \leq \tilde{d}^{(c)}(a^{(m)}, b^{(m)})$ contradicts (27). Therefore $\pi^* = \hat{\pi}$. ■

Proof of Proposition 2: From the Definition 3, we have:

$$P_X(a^{(m)}) = \frac{|\mathcal{D}^{(a^{(m)})}|}{n} = P_X^{\min} + \epsilon, \quad (31)$$

where $n = k - j + 1$ and $\epsilon \geq 0$.

Using (2)

$$\begin{aligned} \tilde{d}^{(c)}(a^{(m)}, u^{(m)}) &= \sum_{i=j}^k \frac{d_0^{(c)}(\{a^{(m)}(i)\}, \{u^{(m)}(i)\})}{n} \\ &= \frac{1}{n} \sum_{i \in \mathcal{D}^{(a^{(m)})}} d_0^{(c)}(\{a^{(m)}(i)\}, \{u^{(m)}(i)\}) + \frac{n - |\mathcal{D}^{(a^{(m)})}|}{n} c \\ &\leq (P_X^{\min} + \epsilon)\epsilon + (1 - P_X^{\min} - \epsilon)c \\ &\leq \epsilon P_X^{\min} + (1 - P_X^{\min})c - \epsilon(c - \epsilon) \\ &\leq \epsilon P_X^{\min} + (1 - P_X^{\min})c. \end{aligned} \quad (32)$$

Similarly we have

$$\tilde{d}^{(c)}(b^{(m)}, u^{(m)}) \leq \epsilon P_X^{\min} + (1 - P_X^{\min})c. \quad \blacksquare$$

B. Pseudocodes

The pseudocode for determining matched pairs based on OSPA⁽²⁾ distance between two tracks is given in Algorithm B.1. The pseudocode for updating matched history for the matched pairs is given in Algorithm B.2. Lastly, the pseudocode for updating consensed labels to ensure label consistency is given in Algorithm B.3.

Algorithm B.1 DetermineMatchedPairs

Input: $\mathbf{T}_k^{(a)}, \mathbf{T}_k^{(b)}$;
Output: $Q_k = [Q_k^{(a)}, Q_k^{(b)}]$;

```

1:  $C := \text{zeros}(|\mathbf{T}_k^{(a)}|, |\mathbf{T}_k^{(b)}|)$ ;  $H^* := \text{zeros}(|\mathbf{T}_k^{(a)}|, |\mathbf{T}_k^{(b)}|)$ ;
2: for  $m = 1 : |\mathbf{T}_k^{(a)}|$  do
3:   for  $n = 1 : |\mathbf{T}_k^{(b)}|$  do
4:      $C_{m,n} := \tilde{d}^{(c)}(a^{(m)}, b^{(n)})$  via (2)
5:   end for
6: end for
7:  $\pi^* := \text{OptimalAssignment}(C)$ ;  $\triangleright$  Use Hungarian's algorithm.
8: for  $m = 1 : |\mathbf{T}_k^{(a)}|$  do
9:    $H_{m, \pi^*(m)}^* := 1$ ;
10: end for
11:  $H^* := H^* \odot (C < C_{\text{match}})$ ;  $\triangleright$  Select assignments with cost  $C < C_{\text{match}}$ .
12:  $i_k^{(a)} := [1 : |\mathbf{T}_k^{(a)}|]^T$ ;  $i_k^{(b)} := [1 : |\mathbf{T}_k^{(b)}|]^T$ ;
13:  $Q_k^{(a)} := i_k^{(a)}$ ;  $Q_k^{(b)} := H^* \cdot i_k^{(b)}$ ;  $Q_k := [Q_k^{(a)}, Q_k^{(b)}]$ ;
14:  $Q_{\text{check}} := [Q_k^{(a)} \odot Q_k^{(b)}] > 0$ ;  $\triangleright$  Ensure  $H_{m, \pi^*(m)}^* = 1$ .
15:  $Q_k := Q_k(\cdot, Q_{\text{check}})$ ;

```

REFERENCES

- [1] S. Blackman and R. Popoli, *Design and analysis of modern tracking systems*. Artech House, 1999.
- [2] J. Mullane, B. Vo, M. D. Adams, and B. Vo, "A random-finite-set approach to Bayesian SLAM," *IEEE Trans. on Robotics*, vol. 27, no. 2, pp. 268–282, April 2011.
- [3] H. V. Nguyen, M. Chesser, L. P. Koh, H. Rezafighi, and D. C. Ranasinghe, "Trackerbots: Autonomous unmanned aerial vehicle for real-time localization and tracking of multiple radio-tagged animals," *J. of Field Robotics*, vol. 36, no. 3, pp. 617–635, 2019.
- [4] I. J. Cox and S. L. Hingorani, "An efficient implementation of Reid's multiple hypothesis tracking algorithm and its evaluation for the purpose of visual tracking," *IEEE Trans. on Patt. Analysis and Machine Intel.*, vol. 18, no. 2, pp. 138–150, Feb 1996.

Algorithm B.2 UpdateMatchedHistory

Input: $\Xi_{1:k-1}^{(a,b)}$; $\mathbf{L}_{1:k}^{(a)}$; $\mathbf{L}_{1:k}^{(b)}$; $Q_k = [Q_k^{(a)}, Q_k^{(b)}]$;
Output: $\Xi_{1:k}^{(a,b)}$;

```

1:  $\Xi_{1:k}^{(a,b)} := \text{zeros}(|\mathbf{L}_{1:k}^{(a)}|, |\mathbf{L}_{1:k}^{(b)}|)$ ;
2:  $\Xi_{1:k}^{(a,b)}(1 : |\mathbf{L}_{1:k-1}^{(a)}|, 1 : |\mathbf{L}_{1:k-1}^{(b)}|) := \Xi_{1:k-1}^{(a,b)}$ ;
3:  $i_{1:k}^{(a)} := 1 : |\mathbf{L}_{1:k}^{(a)}|$ ;  $i_{1:k}^{(b)} := 1 : |\mathbf{L}_{1:k}^{(b)}|$ ;
4: for  $i = 1 : |Q_k^{(a)}|$  do
5:    $m := Q_k^{(a)}(i)$ ;  $n := Q_k^{(b)}(i)$ ;
6:    $\ell^{(m)} := \mathbf{L}_k^{(a)}(\cdot, m)$ ;  $\ell^{(n)} := \mathbf{L}_k^{(b)}(\cdot, n)$ ;
7:    $i_{1:k}^{(m)} := i_{1:k}^{(a)}(\ell^{(m)} = \mathbf{L}_k^{(a)})$ ;
8:    $i_{1:k}^{(n)} := i_{1:k}^{(b)}(\ell^{(n)} = \mathbf{L}_k^{(b)})$ ;
9:    $\Xi_{1:k}^{(a,b)}(i_{1:k}^{(m)}, i_{1:k}^{(n)}) := \Xi_{1:k}^{(a,b)}(i_{1:k}^{(m)}, i_{1:k}^{(n)}) + 1$ ;
10: end for

```

Algorithm B.3 UpdateLabels

Input: $\mathbf{L}_k^{\text{con}}$; $\{\Xi_{1:k}^{(a,b)}\}_{a,b \in \mathcal{N}}$; $\{\mathbf{L}_{1:k}^{(a)}\}_{a \in \mathcal{N}}$;
Output: $\mathbf{L}_k^{\text{con}}$;

\triangleright Create a graph representation using matched history matrices (see label consensus in Section III-E).

```

1:  $G := \text{CreateAGraph}(\{\Xi_{1:k}^{(a,b)}\}_{a,b \in \mathcal{N}})$ ;
2:  $i_{1:k} := 1 : |\{\mathbf{L}_{1:k}^{(a)}\}_{a \in \mathcal{N}}|$ ;
3: for  $i = 1 : |\mathbf{L}_k^{\text{con}}|$  do
4:    $\ell := \mathbf{L}_k^{\text{con}}(\cdot, i)$ ;
5:    $m := i_{1:k}(\ell = \{\mathbf{L}_{1:k}^{(a)}\}_{a \in \mathcal{N}})$ ;
6:    $M := \text{Nearest}(G, m)$ ;  $\triangleright$  Get all connected vertices to vertex  $m$ .
7:    $\text{count} := |M|$ ;
8:   while  $\text{count} > 0$  do
9:      $\text{count} := \text{count} - 1$ ;
10:     $\mathbf{L}^{\text{sel}} := \{\mathbf{L}_{1:k}^{(a)}\}_{a \in \mathcal{N}}(\cdot, M)$ ;
11:     $\triangleright$  Get the smallest index using lexicographical order via (19).
12:     $[\sim, n] := \min(\mathbf{L}^{\text{sel}})$ ;
13:     $\ell' = \mathbf{L}^{\text{sel}}(\cdot, n)$ ;
14:    if  $\ell' \notin \mathbf{L}_k^{\text{con}}$  then  $\triangleright$  Ensure labels' uniqueness.
15:       $\mathbf{L}_k^{\text{con}}(\cdot, i) := \ell'$ ;  $\triangleright$  Update the label.
16:      break;  $\triangleright$  Escape while loop.
17:    end if
18:     $M(n) := []$ ;  $\triangleright$  Remove  $n$  from the nearest vertices.
19:  end while
20: end for

```

- [5] M. Munz, M. Mählich, and K. Dietmayer, "Generic centralized multi sensor data fusion based on probabilistic sensor and environment models for driver assistance systems," *IEEE Intel. Transport. Systems Magazine*, vol. 2, no. 1, pp. 6–17, Spring 2010.
- [6] S. Reuter, A. Danzer, M. Stübler, A. Scheel, and K. Granström, "A fast implementation of the labeled multi-Bernoulli filter using Gibbs sampling," in *IEEE Intel. Veh. Symp.*, 2017, pp. 765–772.
- [7] R. Hoseinnezhad, B.-N. Vo, B.-T. Vo, and D. Suter, "Visual tracking of numerous targets via multi-Bernoulli filtering of image data," *Pattern Recognition*, vol. 45, no. 10, pp. 3625–3635, 2012.
- [8] S. H. Rezafighi, S. Gould, B. T. Vo, B.-N. Vo, K. Mele, and R. Hartley, "Multi-target tracking with time-varying clutter rate and detection profile: application to time-lapse cell microscopy sequences," *IEEE Trans. on Medical Imaging*, vol. 34, no. 6, pp. 1336–1348, 2015.
- [9] E. L. Souza, E. F. Nakamura, and R. W. Pazzi, "Target tracking for sensor networks: A survey," *ACM Computing Surveys*, vol. 49, no. 2, Jun. 2016.
- [10] G. Battistelli, L. Chisci, C. Fantacci, A. Farina, and A. Graziano, "Consensus CPHD filter for distributed multitarget tracking," *IEEE J. of Sel. Topics in Signal Process.*, vol. 7, no. 3, pp. 508–520, 2013.
- [11] G. Battistelli and L. Chisci, "Kullback-Leibler average, consensus on probability densities, and distributed state estimation with guaranteed stability," *Automatica*, vol. 50, no. 3, pp. 707–718, 2014.
- [12] S. Li, G. Battistelli, L. Chisci, W. Yi, B. Wang, and L. Kong, "Computationally efficient multi-agent multi-object tracking with labeled random finite sets," *IEEE Trans. on Signal Process.*, vol. 67, no. 1, pp. 260–275, 2019.
- [13] A. R. Persico, P. Kirkland, C. Clemente, J. J. Soraghan, and M. Vasile, "Cubesat-based passive bistatic radar for space situational awareness:

- A feasibility study," *IEEE Transactions on Aerospace and Electronic Systems*, vol. 55, no. 1, pp. 476–485, Feb 2019.
- [14] Z.-Q. Luo, M. Gastpar, J. Liu, and A. Swami, "Distributed signal processing in sensor networks [from the guest editors]," *IEEE Signal Process. Magazine*, vol. 23, no. 4, pp. 14–15, July 2006.
- [15] R. P. Mahler, *Statistical multisource-multitarget information fusion*. Artech House, Inc., 2007, vol. 685.
- [16] M. E. Liggins, C.-Y. Chong, I. Kadar, M. G. Alford, V. Vannicola, and S. Thomopoulos, "Distributed fusion architectures and algorithms for target tracking," *Proc. of IEEE*, vol. 85, no. 1, pp. 95–107, Jan 1997.
- [17] R. P. Mahler, "Optimal/robust distributed data fusion: a unified approach," in *Signal Process., Sensor Fusion, and Target Recogn. IX*, vol. 4052. Inter. Society for Optics and Photonics, 2000, pp. 128–138.
- [18] M. Üney, D. E. Clark, and S. J. Julier, "Distributed fusion of PHD filters via exponential mixture densities," *IEEE J. of Sel. Topics in Signal Process.*, vol. 7, no. 3, pp. 521–531, June 2013.
- [19] R. P. S. Mahler, "Multitarget Bayes filtering via first-order multitarget moments," *IEEE Trans. on Aerosp. Electron. Systems*, vol. 39, no. 4, pp. 1152–1178, Oct 2003.
- [20] R. Mahler, "PHD filters of higher order in target number," *IEEE Trans. on Aerosp. Electron. Systems*, vol. 43, no. 4, 2007.
- [21] B.-T. Vo, B.-N. Vo, and A. Cantoni, "The cardinality balanced multi-target multi-Bernoulli filter and its implementations," *IEEE Trans. on Signal Process.*, vol. 57, no. 2, pp. 409–423, 2009.
- [22] J. L. Williams, "An efficient, variational approximation of the best fitting multi-bernoulli filter," *IEEE Trans. on Signal Process.*, vol. 63, no. 1, pp. 258–273, Jan 2015.
- [23] S. Reuter, B.-T. Vo, B.-N. Vo, and K. Dietmayer, "The labeled multi-Bernoulli filter," *IEEE Trans. on Signal Process.*, vol. 62, no. 12, pp. 3246–3260, 2014.
- [24] B.-T. Vo and B.-N. Vo, "Labeled random finite sets and multi-object conjugate priors," *IEEE Trans. on Signal Process.*, vol. 61, no. 13, pp. 3460–3475, 2013.
- [25] B.-N. Vo, B.-T. Vo, and D. Phung, "Labeled random finite sets and the Bayes multi-target tracking filter," *IEEE Trans. on Signal Process.*, vol. 62, no. 24, pp. 6554–6567, 2014.
- [26] B.-N. Vo and B.-T. Vo, "A multi-scan labeled random finite set model for multi-object state estimation," *IEEE Trans. on Signal Process.*, vol. 67, no. 19, pp. 4948–4963, 2019.
- [27] T. M. Cover and J. A. Thomas, *Elements of information theory*. John Wiley & Sons, 2012.
- [28] K.-C. Chang, C.-Y. Chong, and S. Mori, "Analytical and computational evaluation of scalable distributed fusion algorithms," *IEEE Trans. on Aerosp. Electron. Systems*, vol. 46, no. 4, pp. 2022–2034, 2010.
- [29] S. J. Julier, T. Bailey, and J. K. Uhlmann, "Using exponential mixture models for suboptimal distributed data fusion," in *Proc. of the IEEE Nonlinear Statistical Signal Process. Workshop*, 2006, pp. 160–163.
- [30] D. Clark, S. Julier, R. Mahler, and B. Ristic, "Robust multi-object sensor fusion with unknown correlations," in *Proc. of the Sensor Signal Process. for Defence*, Sep. 2010, pp. 1–5.
- [31] C. Fantacci, B.-N. Vo, B.-T. Vo, G. Battistelli, and L. Chisci, "Consensus labeled random finite set filtering for distributed multi-object tracking," *arXiv preprint arXiv:1501.01579*, 2015.
- [32] M. B. Hurley, "An information theoretic justification for covariance intersection and its generalization," in *Proc. of the 5th FUSION*, vol. 1, 2002, pp. 505–511.
- [33] B. Wang, W. Yi, R. Hoseinnezhad, S. Li, L. Kong, and X. Yang, "Distributed fusion with multi-Bernoulli filter based on generalized covariance intersection," *IEEE Trans. on Signal Process.*, vol. 65, no. 1, pp. 242–255, 2016.
- [34] C. Fantacci, B.-N. Vo, B.-T. Vo, G. Battistelli, and L. Chisci, "Robust fusion for multisensor multiobject tracking," *IEEE Signal Process. Lett.*, vol. 25, no. 5, pp. 640–644, 2018.
- [35] S. Li, W. Yi, R. Hoseinnezhad, G. Battistelli, B. Wang, and L. Kong, "Robust distributed fusion with labeled random finite sets," *IEEE Trans. on Signal Process.*, vol. 66, no. 2, pp. 278–293, 2018.
- [36] W. Yi, S. Li, B. Wang, R. Hoseinnezhad, and L. Kong, "Computationally efficient distributed multi-sensor fusion with multi-Bernoulli filter," *IEEE Trans. on Signal Process.*, vol. 68, pp. 241–256, 2020.
- [37] M. Üney, J. Houssineau, E. Delande, S. J. Julier, and D. E. Clark, "Fusion of finite-set distributions: Pointwise consistency and global cardinality," *IEEE Trans. on Aerosp. Electron. Systems*, vol. 55, no. 6, pp. 2759–2773, Dec 2019.
- [38] G. Li, G. Battistelli, W. Yi, and L. Kong, "Distributed multi-sensor multi-view fusion based on generalized covariance intersection," *Signal Process.*, vol. 166, p. 107246, 2020.
- [39] T. Li, J. M. Corchado, and S. Sun, "Partial consensus and conservative fusion of gaussian mixtures for distributed phd fusion," *IEEE Trans. on Aerosp. Electron. Systems*, vol. 55, no. 5, pp. 2150–2163, Oct 2019.
- [40] T. Li, M. Mallick, and Q. Pan, "A parallel filtering-communication based cardinality consensus approach for real-time distributed phd filtering," *IEEE Sensors Journal*, pp. 1–1, 2020.
- [41] L. Gao, G. Battistelli, and L. Chisci, "Multiobject fusion with minimum information loss," *IEEE Signal Process. Lett.*, vol. 27, pp. 201–205, 2020.
- [42] T. Li, X. Wang, Y. Liang, and Q. Pan, "On arithmetic average fusion and its application for distributed multi-bernoulli multitarget tracking," *IEEE Trans. on Signal Process.*, vol. 68, pp. 2883–2896, 2020.
- [43] L. Gao, G. Battistelli, and L. Chisci, "Event-triggered distributed multi-target tracking," *IEEE Trans. on Signal and Inf. Process. over Networks*, vol. 5, no. 3, pp. 570–584, Sep. 2019.
- [44] C.-Y. Chong, S. Mori, and K.-C. Chang, "Distributed multitarget multi-sensor tracking," *Multitarget-multisensor tracking: Advanced applications*, pp. 247–296, 1990.
- [45] K. C. Chang, R. K. Saha, and Y. Bar-Shalom, "On optimal track-to-track fusion," *IEEE Trans. on Aerosp. Electron. Systems*, vol. 33, no. 4, pp. 1271–1276, 1997.
- [46] C.-Y. Chong, S. Mori, W. H. Barker, and K.-C. Chang, "Architectures and algorithms for track association and fusion," *IEEE Aerospace and Electronic Systems Magazine*, vol. 15, no. 1, pp. 5–13, 2000.
- [47] S. Mori, W. H. Barker, C.-Y. Chong, and K.-C. Chang, "Track association and track fusion with nondeterministic target dynamics," *IEEE Trans. on Aerosp. Electron. Systems*, vol. 38, no. 2, pp. 659–668, 2002.
- [48] S. Mori and C.-Y. Chong, "Track-to-track association metric I.I.D.-non-Poisson cases," in *Proc. of the 6th International Conference of Information Fusion*, vol. 1, July 2003, pp. 553–559.
- [49] L. M. Kaplan, Y. Bar-Shalom, and W. D. Blair, "Assignment costs for multiple sensor track-to-track association," *IEEE Trans. on Aerosp. Electron. Systems*, vol. 44, no. 2, pp. 655–677, 2008.
- [50] S. Mori, K. Chang, and C. Chong, "Performance prediction of feature-aided track-to-track association," *IEEE Trans. on Aerosp. Electron. Systems*, vol. 50, no. 4, pp. 2593–2603, 2014.
- [51] X. Tian, T. Yuan, and Y. Bar-Shalom, "Track-to-track fusion in linear and nonlinear systems," in *Advances in Estimation, Navigation, and Spacecraft Control*. Berlin, Heidelberg: Springer Berlin Heidelberg, 2015, pp. 21–41.
- [52] M. Beard, B. T. Vo, and B.-N. Vo, "OSPA⁽²⁾: using the OSPA metric to evaluate multi-target tracking performance," in *Proc. of the 7th ICCAIS*, Oct 2017, pp. 86–91.
- [53] M. Beard, B. T. Vo, and B. Vo, "Performance evaluation for large-scale multi-target tracking algorithms," in *Proc. of the 21st FUSION*, July 2018, pp. 1–5.
- [54] —, "A solution for large-scale multi-object tracking," *IEEE Trans. on Signal Process.*, pp. 1–16, 2020.
- [55] D. Schuhmacher, B.-T. Vo, and B.-N. Vo, "A consistent metric for performance evaluation of multi-object filters," *IEEE Trans. on Signal Process.*, vol. 56, no. 8, pp. 3447–3457, 2008.
- [56] H. W. Kuhn, "The Hungarian method for the assignment problem," *Naval research logistics quarterly*, vol. 2, no. 1-2, pp. 83–97, 1955.
- [57] J. Munkres, "Algorithms for the assignment and transportation problems," *J. of the society for industrial and applied mathematics*, vol. 5, no. 1, pp. 32–38, 1957.
- [58] N. Tomizawa, "On some techniques useful for solution of transportation network problems," *Networks*, vol. 1, no. 2, pp. 173–194, 1971.
- [59] J. Edmonds and R. M. Karp, "Theoretical improvements in algorithmic efficiency for network flow problems," *J. of the ACM (JACM)*, vol. 19, no. 2, pp. 248–264, 1972.
- [60] R. Jonker and A. Volgenant, "A shortest augmenting path algorithm for dense and sparse linear assignment problems," *Computing*, vol. 38, no. 4, pp. 325–340, 1987.
- [61] D. Reid, "An algorithm for tracking multiple targets," *IEEE Trans. on Automatic Control*, vol. 24, no. 6, pp. 843–854, 1979.
- [62] B. Ristic, B.-T. Vo, B.-N. Vo, and A. Farina, "A tutorial on bernoulli filters: theory, implementation and applications," *IEEE Transactions on Signal Processing*, vol. 61, no. 13, pp. 3406–3430, 2013.
- [63] B.-N. Vo, B.-T. Vo, and H. G. Hoang, "An efficient implementation of the generalized labeled multi-Bernoullifilter," *IEEE Trans. on Signal Process.*, vol. 65, no. 8, pp. 1975–1987, 2016.
- [64] L. Xiao, S. Boyd, and S. Lall, "A scheme for robust distributed sensor fusion based on average consensus," in *Proc. of the 4th IPSN*, 2005, pp. 63–70.
- [65] J. R. Hoffman and R. P. S. Mahler, "Multitarget miss distance via optimal assignment," *IEEE Trans. on Systems, Man, and Cybernetics - Part A: Systems and Humans*, vol. 34, no. 3, pp. 327–336, 2004.